



HAL
open science

Quality index for Martian in-situ laser-induced breakdown spectroscopy data

Zhaopeng Chen, Olivier Forni, Agnès Cousin, Paolo Pilleri, Olivier Gasnault, Sylvestre Maurice, Roger Wiens, Yizhong Zhang, Yuxuan Luo, Xin Ren, et al.

► To cite this version:

Zhaopeng Chen, Olivier Forni, Agnès Cousin, Paolo Pilleri, Olivier Gasnault, et al.. Quality index for Martian in-situ laser-induced breakdown spectroscopy data. *Spectrochimica Acta Part B: Atomic Spectroscopy*, 2024, 216, pp.106921. 10.1016/j.sab.2024.106921 . hal-04784251

HAL Id: hal-04784251

<https://hal.science/hal-04784251v1>

Submitted on 14 Nov 2024

HAL is a multi-disciplinary open access archive for the deposit and dissemination of scientific research documents, whether they are published or not. The documents may come from teaching and research institutions in France or abroad, or from public or private research centers.

L'archive ouverte pluridisciplinaire **HAL**, est destinée au dépôt et à la diffusion de documents scientifiques de niveau recherche, publiés ou non, émanant des établissements d'enseignement et de recherche français ou étrangers, des laboratoires publics ou privés.



Distributed under a Creative Commons Attribution 4.0 International License



Contents lists available at ScienceDirect

Spectrochimica Acta Part B: Atomic Spectroscopy

journal homepage: www.elsevier.com/locate/sab

Quality index for Martian in-situ laser-induced breakdown spectroscopy data

Zhaopeng Chen^{a,b,c,*}, Olivier Forni^b, Agnès Cousin^b, Paolo Pilleri^b, Olivier Gasnault^b, Sylvestre Maurice^b, Roger C. Wiens^d, Yizhong Zhang^{a,c}, Yuxuan Luo^{a,c}, Xin Ren^a, Weiming Xu^e, Xiangfeng Liu^e, Rong Shu^e, Chunlai Li^a

^a Key Laboratory of Lunar and Deep Space Exploration, National Astronomical Observatories, Chinese Academy of Sciences, 20A Datun Rd., Beijing 100101, China

^b Institut de Recherche en Astrophysique et Planétologie, Université de Toulouse, UPS, CNRS, 9 avenue du Colonel Roche, Toulouse 31400, France

^c School of Astronomy and Space Sciences, University of Chinese Academy of Sciences, 19A Yuquan Rd., Beijing 100049, China

^d Earth, Atmospheric, and Planetary Sciences, Purdue University, 610 Purdue Mall, West Lafayette, 47906 Indiana, USA

^e Shanghai Institute of Technical Physics, Chinese Academy of Sciences, 500 Yutian Rd., Shanghai 200083, China

ARTICLE INFO

Keywords:

Laser-induced breakdown spectroscopy
Data quality
Mars exploration
Mars atmosphere

ABSTRACT

Laser-induced breakdown spectroscopy (LIBS) has been widely implemented in Mars explorations as a versatile technique for in-situ chemical analysis. Determination of elemental composition from Martian LIBS typically relies on uni/multi-variate models trained on specific laboratory datasets, which in turn requires similarities between this training dataset and Martian data. However, plasma excitation can affect this similarity. The inability to identify insufficiently excited data may ignore poor focusing for some observations or lead to unawareness of compositional uncertainty. This study establishes the LIBS Quality Index (LQI) for Martian LIBS data quality by evaluating the carbon ionic doublet emission around 658 nm for the Martian atmosphere, assessing its signal-to-noise ratio as well as its deviation from the line profile standard of the instrument-specific laboratory dataset. This method allows the LQI to be used as a confidence level for assessing LIBS excitation quality and measurement for similarity with instrument-specific laboratory datasets. The LQI evaluation routines were established for ChemCam, MarSCoDe, and SuperCam. Validation of LQI was carried out on the laboratory datasets and Mars data with known quality assessments of the three instruments. The index was verified to be sensitive to input irradiance, applicable with three current Mars LIBS instruments, robust against various material types (except carbonate), and moderate interference from H, Fe, and Ti. Applying the LQI, the study was able to identify the remote micro-imager (RMI) autofocus as an optimal mechanism, to discover the influence of environmental conditions on data quality, to discuss the impact of target material consolidation and morphology on data quality, and to investigate the contribution of data quality to quantification uncertainty. These application examples demonstrated the feasibility of LQI as a useful and sensitive tool to assess data quality and its potential to aid current and future Martian LIBS explorations.

1. Introduction

In-situ laser-induced breakdown spectroscopy (LIBS) has been widely implemented in robotic Martian exploration as a versatile technique to remotely detect elemental compositions on the Martian surface, e.g., ChemCam [1,2] (MSL Curiosity rover, NASA, 2011), SuperCam [3,4] (Mars2020 Perseverance rover, NASA, 2020), and MarSCoDe [5] (Tianwen-1 Zhurong rover, CNSA, 2020). Current Martian in-situ LIBS

typically employs an MW-infrared pulsed laser, a telescope, and spectrometers to create and observe a laser-induced plasma on a Mars target at a 1–7 m distance, with possible co-axial instruments like micro-imager, passive reflectance spectrometer, or Raman spectroscopy suite to further characterize the target texture and mineralogy. Its observation procedure does not require additional sample preparation and can be automated (e.g., AEGIS [6]). LIBS-included suites have played important roles in their corresponding missions by acquiring a considerable

* Corresponding author at: Key Laboratory of Lunar and Deep Space Exploration, National Astronomical Observatories, Chinese Academy of Sciences, 20A Datun Rd., Beijing 100101, China.

E-mail address: chenzp@nao.cas.cn (Z. Chen).

<https://doi.org/10.1016/j.sab.2024.106921>

Received 18 September 2023; Received in revised form 2 March 2024; Accepted 9 April 2024

Available online 12 April 2024

0584-8547/© 2024 The Authors. Published by Elsevier B.V. This is an open access article under the CC BY license (<http://creativecommons.org/licenses/by/4.0/>).

amount of data which has helped to understand the geological contexts (e.g., Refs. [7–9]).

The inference of element compositions from LIBS spectra is based on the principles of atomic emission spectroscopy (AES), where the intensities of atomic or ionic emissions in the plasma are related to the concentration of the corresponding element. However, considering the practical situation of the LIBS technique and unknown Martian conditions, factors like short plasma lifetime, uncontrolled environment, and target matrix effect may deviate the relationship from ideal AES in the local thermal equilibrium (LTE) condition, thus rendering the elemental composition calibration much more difficult [10–14]. Consequently, the current practices of elemental calibration (especially for major elements) for Martian LIBS usually prefer multi-variate machine learning approaches, where case-specific training data is employed to optimize a modeled relationship between spectral intensities and elemental concentrations: Major Oxide Composition (MOC) of ChemCam rely on a combination of partial least square (PLS) regression and independent component analysis (ICA) [15,16]; The models that established for SuperCam MOC take an ensemble learning approach by combinations of algorithms, including gradient boosting regression (GBR), Lasso regression, PLS, and random forest regression, that achieves optimal performance on different elements [17]; probabilistic major element composition (PMEC) for MarSCoDe incorporated natural gradient boosting (NGBoost [18]) for quantification with dynamic uncertainty estimation [19], and studies also suggest that methods such as artificial neural network (e.g., Refs. [20–23]), transfer-learning (e.g., Refs. [22–25]), etc. could provide calibrations.

While benefiting from the complexity provided by the algorithms, machine learning calibrations require a similarity between the input Mars data and the training data [26,27]. In terms of LIBS data, we suggest that the data similarity generally has three aspects: 1) instrument response, 2) material types (related to composition and chemical/physical matrix effect), and 3) plasma excitation. Instrument response includes response functions, instrumental spectral resolution, wavelength alignment, etc., which are determined by the optics and electronics themselves. The instrumental response is usually calibrated to be consistent in practice. Material type similarity implies that the training set must cover a range of materials to be prepared for Martian data with unknown composition and matrix effect. Efforts to achieve this similarity have been extensive for Mars LIBS campaigns [16,17,19].

The last aspect, plasma excitation, corresponds to the similarity of the laser conditions (e.g., pulse duration, laser power) and the on-target irradiance (focus condition). The laser usually remains controlled during the operation, but the latter can vary. Inaccuracy of the focusing mechanism or rapid removal of loose material [19,28] can lead to a loss of focus and insufficient excitation of the plasma, inducing line-dependent changes to emission features and thus deviating the Mars data from the training dataset. Plasma excitation characterization is therefore important for Mars LIBS operation. Identifying data with insufficient excitation can help attribute additional uncertainty to composition results and recognize potential inaccuracy in the focus mechanism.

However, a tool to reliably assess the quality of the plasma excitation of Mars LIBS data is not yet available. The precise determination of LTE plasma parameters like temperature and electron density is not possible with the current Mars LIBS instrument due to the lack of precise time gating [1–5,29]. The total emission of LIBS spectra is sometimes used to filter out low-quality data (e.g., in the SuperCam data inventory in the Planetary Data System (PDS) [30]) but it is dependent on material properties (also discussed later in Section 3.2). Previous work by Chen et al. [19] has introduced the potential of atmospheric carbon ionic emission around 658 nm (abbr. C-658) as a figure of merit for excitation quality, mostly composition-independent. The work was continued in Ref. [31] to formulate the LIBS Quality Index (LQI), a composite evaluation of C-658 peak signal-to-noise ratio and line shape for LIBS instruments on Mars. In this work, the authors have further refined the LQI

methodology, optimized its robustness, and discussed its applicability and potential application on current Martian LIBS operations.

2. Defining a LIBS quality index

2.1. Theory on C-658 as an indicator of input irradiance

The Martian atmosphere is characterized by its CO₂-dominated composition, which provides a ubiquitous source of carbon and oxygen atoms to interact with the laser-induced plasma. Meanwhile, Martian soil and rocks are not generally carbon-rich [32,33]. Thus, the presence of carbon in LIBS data can be considered material-independent in the absence of carbonate occurrences. The LQI to be presented is derived from the C-658 emission using standard spectra from the laboratory dataset. The choice of C-658 is based on the fact that the emission is a sensitive indicator of input irradiance. This is determined by how CO₂ interacts with the plasma, as explained in the simplified procedure below:

- 1) The laser first vaporizes and excites the solid material around its focus, where little CO₂ is directly excited by the laser due to a higher breakdown threshold of the gas [11]. Here we consider only the electron as the main energy transfer agent and simplify the process to inverse-Bremsstrahlung only [10]:

$$e^-(\varepsilon) + ah\nu \rightleftharpoons e^-(\varepsilon + \alpha) \quad (1)$$

where ε is considered an undistinguished base kinetic energy of an electron and α is the excess kinetic energy.

- 2) The expanding plasma comes into contact with the atmosphere. CO₂ is atomized and excited by the electron in this contact process:

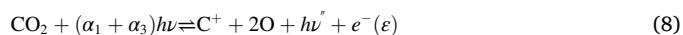


where α_1 represents a molecular bonding energy of CO₂ (about 4 eV, calculated from the enthalpy of formation for CO₂ at 298 K [34]), α_2 represents the neutral line energy levels of carbon atom (e.g., 5.00 eV for C I 247.856 nm emission [35]), α_3 represents a sum of the carbon first ionization energy (11.26 eV [34]) and the ionic line energy level (about 1.88 eV for C-658) [35].

- 3) Excited carbon species emit atomic and ionic lines:



The above reactions can be combined by stoichiometry into:



We assume that there is no self-absorption and that each reaction is simply controlled by the probability of repeated collisions among species and photons, which allows the reaction rates of Eq. 7 and Eq. 8 to be formulated as power laws, as follows:

$$I(h\nu') \propto p(\text{CO}_2)I(h\nu)^{\alpha_1 + \alpha_2} \quad (9)$$

$$I(h\nu'') \propto p(\text{CO}_2)I(h\nu)^{\alpha_1 + \alpha_3} \quad (10)$$

Thus, the line intensity of the ionic carbon emission can be considered a more sensitive indicator to input irradiance than the neutral one,

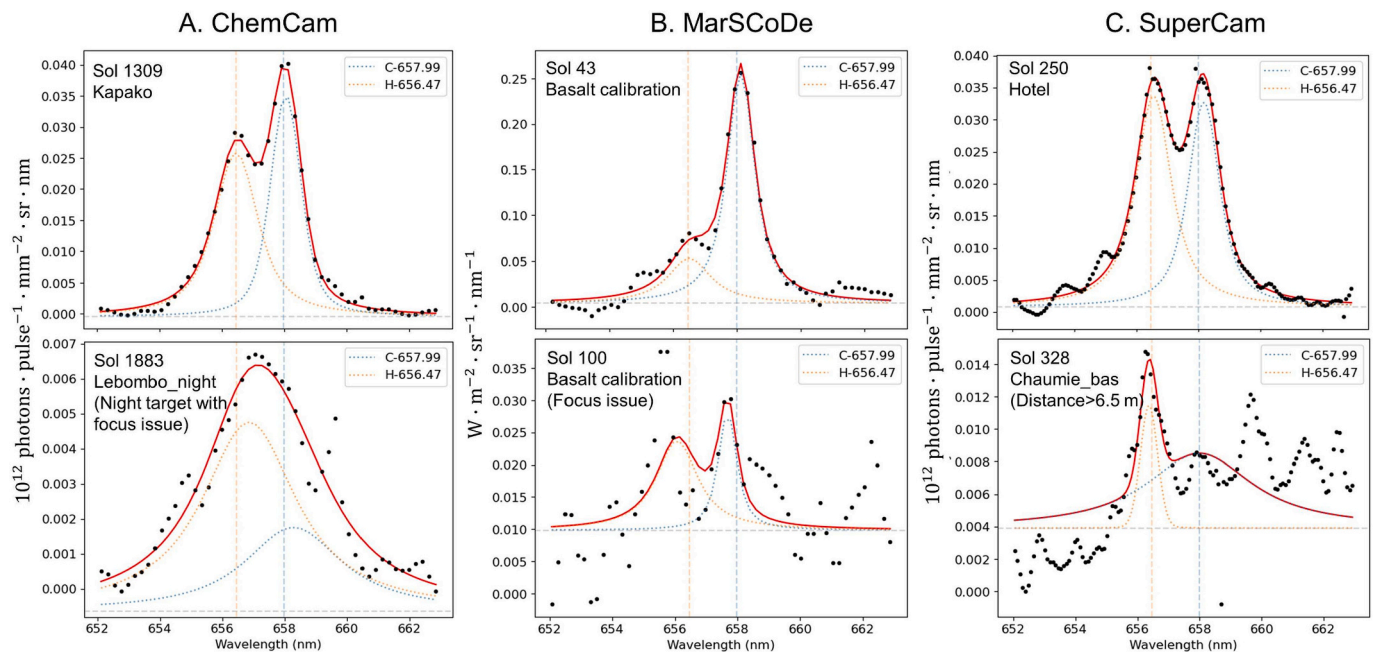


Fig. 1. Examples of C-658 spectral regions (652–663 nm) from ChemCam, MarSCoDe, and SuperCam data of "good" (first row) and "poor" (second row) quality. Original data points are shown as black dots. The acquiring sol (Martian solar day since the landing of the spacecraft), target name, and reason for "poor" quality (second row only [19,30,39]) are indicated in each panel. Preliminary double Voigt fittings (red line) have been applied based on Eq. 11 to highlight the C-658 (dotted and dashed yellow line) and H_{α} (dotted and dashed blue line) emissions. The fitted baselines are shown as dashed grey lines. (For interpretation of the references to colour in this figure legend, the reader is referred to the web version of this article.)

as $\alpha_3 > \alpha_2$. The exact emission is also influenced by the atmospheric pressure (annual variation around 200 Pa [9,36,37]) and, in reality, also by the target composition (e.g., non-electron energy transfer [10]). They were later found to be practically less influential in the evaluation and application of the LQI (Section 3.1).

2.2. LIBS quality evaluation with C-658

According to the established theory, the evaluation of the ionic carbon emission can be indicative of the input irradiance and hence of the data quality. Here, we focus on the C-658 doublet formed by ionic carbon lines at 657.805 and 658.288 nm (C II, $2s^23s - 2s^23p, 2s^2P^{\circ}$, wavelengths in vacuum [35]). Two pieces of information can be extracted from the emission: intensity and line profile. The intensity is directly related to $I(h\nu')$ and the line profile ideally consists of instrumental and physical broadening which together form a Voigt profile with Gaussian (e.g., instrumental, Doppler broadening) and Lorentzian (e.g., Zeeman, Stark broadening) components [10,38]. Practically, as shown in Fig. 1, known "poor" quality LIBS spectra from Mars tend to show weak C-658 signals, with visually low signal-to-noise ratios (SNRs) or distorted line profiles.

To describe the C-658 emission, we incorporate multiple Voigt fits ($V(\lambda)$, the convolution of a Gaussian profile and a Lorentzian profile) around the corresponding spectral region from 652 nm to 663 nm. The main fit includes C-658 and the neighboring H_{α} as:

$$M(\lambda) = A_H \times V(\lambda; \mu_H, \gamma_H, \sigma_H) + A_C \times V(\lambda; \mu_C, \gamma_C, \sigma_C) + B, \quad (11)$$

where $A_i, \mu_i, \gamma_i, \sigma_i (i \in \{C, H\})$, and B represent the line height, line center, Lorentzian scale parameter, Gaussian standard deviation, and baseline, respectively. Certain constraints are added to the fit: 1) limiting μ_C around 657.99 ± 0.3 nm according to the local pixel resolution; 2) fixing μ_H with $\mu_H/\mu_C = 1.00231$ as a physical constraint; 3) fixing σ_C, σ_H using presumed local instrumental full-width half maximum (FWHM), as the Doppler broadening for C and H are generally negligible [10].

The fitting region of this model also contains several interfering iron

emissions that may come with iron-rich material common on Mars [40]. Therefore, before the main fit, there are two possible methods to reduce the iron influences:

- A) Iron lines removal: This measure pre-fits the spectra with additional iron lines and removes the fitted interfering lines from the original data (see Fig. S1). Pre-fitted and removed lines and their specific constraints can be found in the Appendix A.1.
- B) Fitting zone clipping: Another simple measure is to cut the fitting zone into 654–660 nm, due to fitting numerous lines in the previous measure may include uncertainty in subsequent fitting, which practically happened for MarSCoDe.

The main fit is then performed on the Fe-suspended data. The fitting is bootstrapped 10 times by noise-adding to produce stable means and standard deviations of fitted parameters based on local noise (an example without this bootstrapping is shown in Appendix A.2). 10 Gaussian noise templates with a unit amplitude were pre-generated and used for every bootstrapping to ensure the repeatability of the results. The actual noise amplitude to multiply the templates is the maximum of 1) the 3-sigma clipped standard deviation from 550 to 760 nm (the methodology is the same as the sigma clipping in Ref. [15]); 2) the fitted standard deviation of A_C ; 3) the maximum absolute value among the fitting residuals. 2) and 3) are obtained in a separate main fit without noise-adding.

The fitting results produce the signal-to-noise ratio (SNR, Z_A) and its line shape score (Z_{γ}) of C-658. Z_A is given by bootstrapped average values of A_C (\bar{A}_C) and their standard deviation (ΔA_C):

$$Z_A = \bar{A}_C / \Delta A_C \quad (12)$$

and Z_{γ} is given by comparing the bootstrapped average value of γ_C with a standard distribution of the C-658 Lorentzian width (in a Gaussian form centered at Γ_C and with a standard deviation $\Delta \Gamma_C$):

$$Z_{\gamma} = |\gamma_C - \Gamma_C| / \Delta \Gamma_C \quad (13)$$

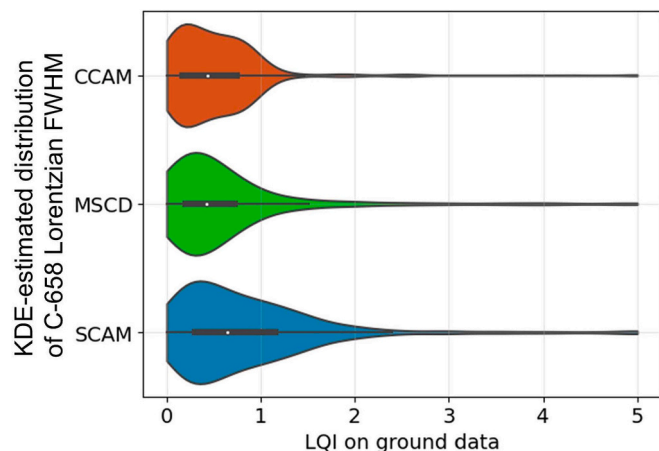


Fig. 2. Distributions of Lorentzian full-width half maxima (FWHM) of C-658 from different LIBS instruments: CCAM for ChemCam, MSCD for MarSCoDe, and SCAM for SuperCam. The values were obtained from the same main fit procedure and corresponding treatments and constraints provided in Fig. 3 and Table 1. For violin plots, the kernel density estimation (KDE) with a bandwidth following Scott's Rule [42] was used to generate smooth distributions.

This formulation is based on the practical discovery of consistent, unimodally distributed C-658 Lorentzian widths among LIBS spectra in the laboratory Mars atmosphere for each LIBS instrument (Fig. 2). A deviation in the Lorentzian width, i.e., a high Z_γ , could indicate an anomaly in the line profile of C-658 as the emission weakens, which may originate from the local disruption to the peak fitting or the potential change in the physical broadening [10,41]. This anomaly is quantified by its deviation from the standard established on the laboratory datasets ($\Gamma_C \pm \Delta\Gamma_C$), which has already taken into account the possible variation in the physical broadening when ablating Mars-like materials with well-focused laser (see the laboratory data description in the Appendix A.3).

The score of the line shape (Z_γ) thus also facilitates the evaluation of the similarity between the laboratory data and the Martian data.

The LIBS Quality Index (LQI) is formulated by combining both of the scores probabilistically. The established scores for SNR and line shape can be used to define the probability of two events:

- Event A: C-658 is significantly above noise, $P(A) = f(Z_A)$;
- Event B: The Lorentzian width of C-658 is not significant deviated from the laboratory dataset, $P(B) = 1 - f(Z_\gamma)$.

$f(n)$ here is the integral of a standard Gaussian distribution between $\pm n$. Both of the events being true (AB) means a "well-forming" C-658 emission. We designate the LQI to characterize the inverse of the events: the probability of either the event being false ($P(\bar{A}\bar{B})$), to better quantify the situation with "poor" data quality:

$$LQI = f^{-1}[P(\bar{A}\bar{B})] = f^{-1}\{1 - f(Z_A) \times [1 - f(Z_\gamma)]\} \quad (14)$$

The procedure to produce LQI is summarized in Fig. 3. The LQI is established for all three Mars LIBS instruments (ChemCam, MarSCoDe, and SuperCam) with their instrument-specific parameters, as shown in Table 1.

3. Results and discussion

3.1. Interpretation and validation of LQI

3.1.1. Interpreting from laboratory datasets

The LQI values were first generated on the laboratory datasets of ChemCam [16], MarSCoDe [19], and SuperCam [17] (carbon-rich and Ti-rich targets were removed). As the laboratory datasets were used as "standards" for the line shape score (Z_γ), their corresponding LQI values are expected to be low. The LQI distributions for the three instruments are shown in Fig. 4a. The influence of SNR (Z_A) can be seen as the distributions are not perfectly centered at LQI = 0 but still with the majority

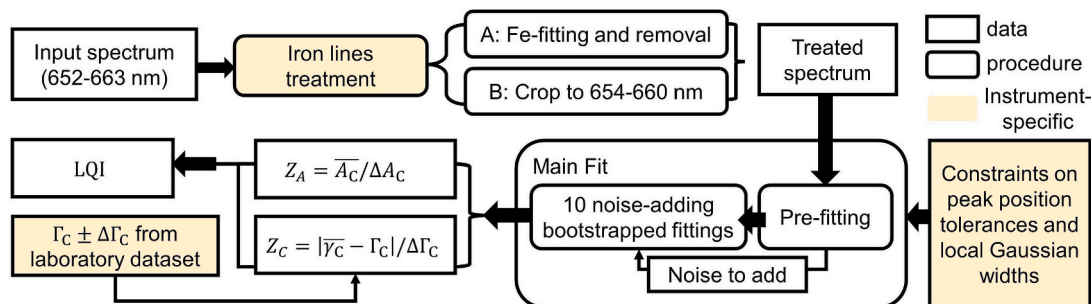


Fig. 3. Flowchart of the procedures and data required to calculate LQI for a LIBS spectrum. Yellow-filled instrument-specific options are further clarified in Table 1 for all three Mars LIBS instruments (ChemCam, MarSCoDe, and SuperCam). (For interpretation of the references to colour in this figure legend, the reader is referred to the web version of this article.)

Table 1

Table of instrument-specific parameters for LQI calculation. C-658 position tolerances are chosen to be larger than local pixel resolutions. Local Gaussian sigmas are obtained from either free-Voigt fitting for the C-658 line (ChemCam), free-Voigt fitting for neighboring lines (MarSCoDe, specifically Si II 637.312 nm, and K I 766.701 nm), or standard lamp lines FWHM (SuperCam [4]). The Gaussian sigma estimations were not expected to be the very exact instrumental broadenings but they were practically adequate as fitting constraints.

Instrument-specific parameters around C-658	Instruments		
	ChemCam	MarSCoDe	SuperCam
Local pixel resolution (nm/pixel)	0.20	0.19	0.08
C-658 position tolerance (nm)	0.3	0.3	0.3
Local Gaussian sigma (nm)	0.37	0.15	0.25
Iron lines treatment	Iron lines removal	Fitting zone clipping	Iron lines removal
Γ_C (nm)	0.34	0.54	0.57
$\Delta\Gamma_C$ (nm)	0.085	0.10	0.10

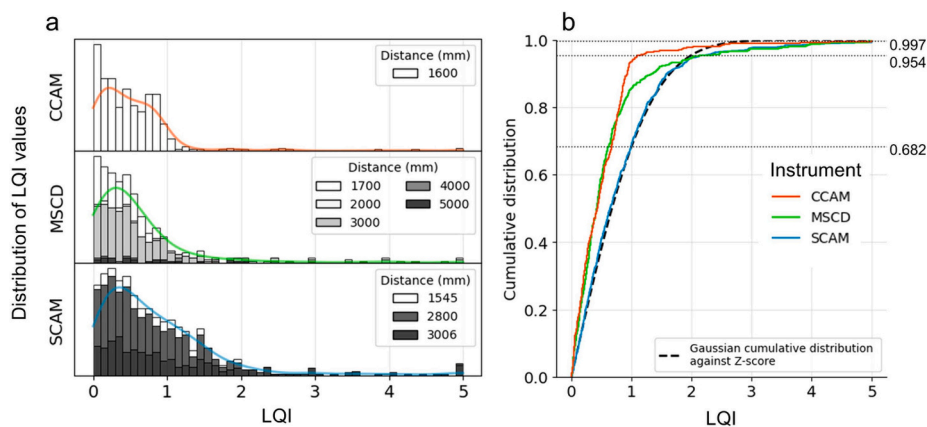


Fig. 4. a) Distributions of LQI values from laboratory datasets of three Martian LIBS instruments. KDE setting is the same as Fig. 2. For SuperCam, several distances around 2800 mm were plotted into one category. The Pearson correlations between distances and LQI values for MarSCOde and SuperCam are 0.18 and 0.07, respectively. b) Cumulative LQI distributions from laboratory datasets of Martian LIBS instruments. $f(n)$ from Eq. 14 is plotted in black dashed line. 68.2%, 95.4%, and 99.7% percentages are highlighted with horizontal dotted lines.

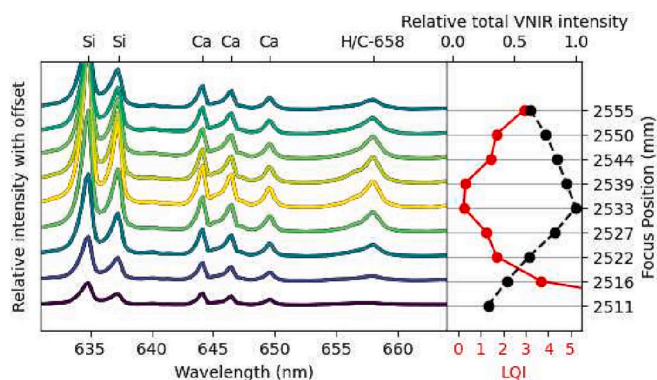


Fig. 5. A showcase of LQI on ChemCam Z-stack on Sol 869 (first Z-stack on target Mojave_Chunks). The mean spectrum of shot #25 to #30 from each step is shown on the left, with colors indicating relative VNIR intensities. LQI values and total VNIR intensities are compared on the right, where median LQI values from shot #25 to #30 of the steps were used. Infinite LQI values were re-assigned as 10. It is worth noting that the ratios among Si and Ca lines were visually altered upon the loss of focus, signifying how plasma excitation affects the spectral features.

of targets in $LQI < 1$ as suggested by their cumulative distributions in Fig. 4b.

The distributions in Fig. 4 also demonstrate the insensitivity of LQI to material and distance within the laboratory datasets. The insensitivity is largely due to the incorporation of $\Delta\Gamma_C$ in the calculation which covered the spectral variations in the laboratory dataset. As the datasets are designed to mimic the Martian composition, this material insensitivity can thus be inherited for its application on Mars. On the other hand, the distance insensitivity is only limited to the laboratory dataset ranges around 1.6–3 m. The C-658 emission of further targets could be controlled by the decreasing irradiance over distance which negatively affects the data quality (later described in Section 3.1.2 and Section 3.1.5).

As designed, LQI can also be interpreted as a measure of similarity with the laboratory dataset. From Fig. 4b, we have discovered that the Z-score interpretation provides a lower limit for the percentage of similar data found in the laboratory dataset when $LQI < 2$, and an upper limit otherwise. For example, with an LQI in the range from 0 to 1, one could infer that the excitation is similar to at least 68% targets of the laboratory dataset; on the other hand, an LQI ranging from 2 to 3 could suggest that at most 4% of the targets in the laboratory dataset are found similar.

The similarity inference here could help qualify the possible uncertainty appearing in the quantification models trained on the laboratory dataset.

3.1.2. Validating with Z-stack data

The interpretation of LQI needs to be justified by a non-laboratory dataset with known excitation quality. A LIBS data sequence with deliberate focus offsets scanning around the best focus, known as Z-stack data [28], is ideal for such validation. During the ChemCam operation in its Season 2 (Sol 815 to 980 [43]), the degradation of the focus-assisting continuous wave laser (CWL) drove the development of a new focusing strategy by Remote-Micro Imager (RMI) [28]. One legacy of the campaign is a number of LIBS data with Z-stack, where the several steps of focus position were scanned near the target surface and each step consisted of 30 shots.

We calculate the LQIs for these Z-stack data (for data processing and selection, see Appendix A.3) to check whether the LQI can identify well-focused steps and compare the results with the integrated count of the visible and near-infrared spectrometer (abbr. VNIR intensity) [2]. A representative Z-stack is shown in Fig. 5, where the LQI minimum is aligned with the VNIR intensity maximum.

The validation was further performed en masse in Season 2 data. For each Z-stack, the VNIR intensities were divided by their maximum so that the best focus position for each Z-stack has a relative VNIR intensity value of 1.0. Two kinds of LQI statistics from each stack were compared with the corresponding relative VNIR intensities: the median LQI from shot #25 to #30 (Fig. 6a) and the single LQI of the #25 shot (Fig. 6b). Qualitatively, the LQI is well-correlated to the relative VNIR intensity as low LQI values co-occur with high relative VNIR intensity, signifying that the LQI is indicative of the focus quality. This was further validated by a quantitative test: using the Z-score empirical rule on LQI (filtering the data with $LQI < 1, 2$, or 3) to identify the good focus steps with relative VNIR intensity > 0.8 . The test was evaluated by its positive and negative predictive values (PPV and NPV), i.e., the accuracy of identifying well-focused and off-focus steps, respectively:

$$PPV = \frac{\text{Number of true positives (relative VNIR} > 0.8 \text{ and } LQI < n)}{\text{Number of positive calls (} LQI < n)}$$

$$NPV = \frac{\text{Number of true negatives (relative VNIR} \leq 0.8 \text{ and } LQI \geq n)}{\text{Number of negative calls (} LQI \geq n)}$$
(15)

The test resulted in 80% PPV for using median LQI < 1 to identify the steps with relative VNIR intensity > 0.8 and 83% NPV for using median LQI ≥ 3 to identify the steps with relative VNIR intensity ≤ 0.8 .

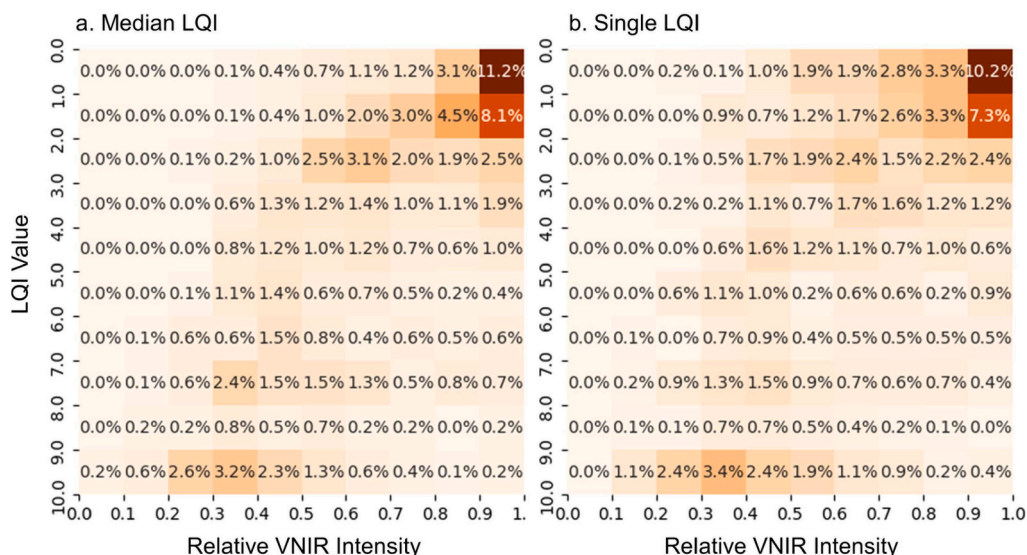


Fig. 6. Heatmaps for the distribution of ChemCam Season 2 Z-stack data over their LQI values and relative VNIR intensity. a) The distribution of Z-stack data based on the median LQI value from shot #25 to #30; b) the distribution based on the single-shot LQI values of shot #25.

The results demonstrate that a low threshold (e.g., $LQI < 1$) practically performs better for selecting well-excited data. On the other hand, a high threshold is sufficient to filter out a target or certain shots with clearly low excitation. The comparison made in Table 2 also shows that the median LQI over a sequence of shots is more representative of the data quality of the entire observation than the single-shot LQI. However, the median LQI should be used with caution in case the target may not be homogeneous or the material ablation by the laser may cause defocusing.

The test on Z-stack data also validated the general robustness of the LQI in the real Mars condition, as all the spectra were obtained from natural targets on Mars. Still, there are some specific "misidentified" examples where high LQI values, thus implying "poor" excitation, are accompanied by high relative VNIR intensities. These data and their corresponding Z-stacks were manually examined and three situations were found: 1) far targets (around 4 to 6 m); 2) Ti-rich targets; and 3) unconsolidated/hydrated targets. Three examples of these situations can be found in Fig. S3. High LQI values at well-focused far targets are expected since these targets have gone out of the distance range of the laboratory dataset (1.6 m for ChemCam) and received low input laser

irradiance. This deviates the spectra from the excitation quality defined by the laboratory dataset. Thus it should be noted that, in this long-distance case, the terms well-focused and well-excited are not equivalent from the perspective of LQI. Titanium or strong hydrogen interference may bring some uncertainty to the fitting of C-658 and thus limit the LQI's applicability on high-Ti or hydrated targets. The robustness of LQI against these interferences is subsequently discussed in Section 3.1.5. Unconsolidated materials can also pose a challenge to the focusing itself and are later found to have worse excitation than solid targets in Section 3.3.3.

3.1.3. The LQI thresholding technique

Based on the aforementioned Z-score interpretation of LQI, LQI distributions on laboratory datasets, and its validation on ChemCam Season 2 data, we propose an LQI thresholding technique to evaluate the LIBS excitation quality of Martian LIBS data and to qualify Martian data similarity compared to laboratory datasets, as formulated in Table 3. The evaluation by the LQI is probabilistic as the LQI itself is defined as a statistical confidence level. Therefore, $LQI < 1$ and $LQI > 3$ are high-confidence criteria for well-excited and outlier data, respectively. An

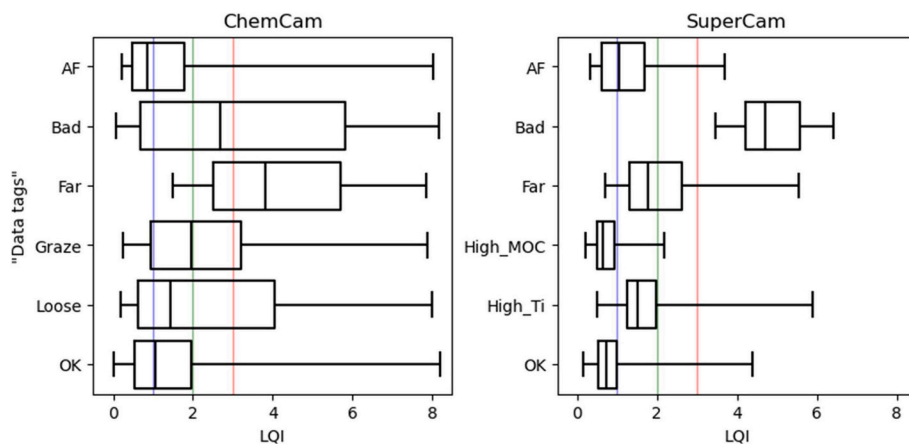


Fig. 7. Distributions of LQI values of the Mars LIBS observations categorized by "data tags" for ChemCam and SuperCam. For the definition of each "tag", see Section 3.1.4. The LQI distribution for each "tag" is described by a horizontal box plot where the whiskers indicate the maximum and minimum values, and the vertical bars in the box, from left to right, represent the first, second, and third quartiles. LQI values were calculated per observation by taking the median of the LQI of all repeated shots in an observation. For all panels, $LQI = 1, 2, 3$ are marked vertically.

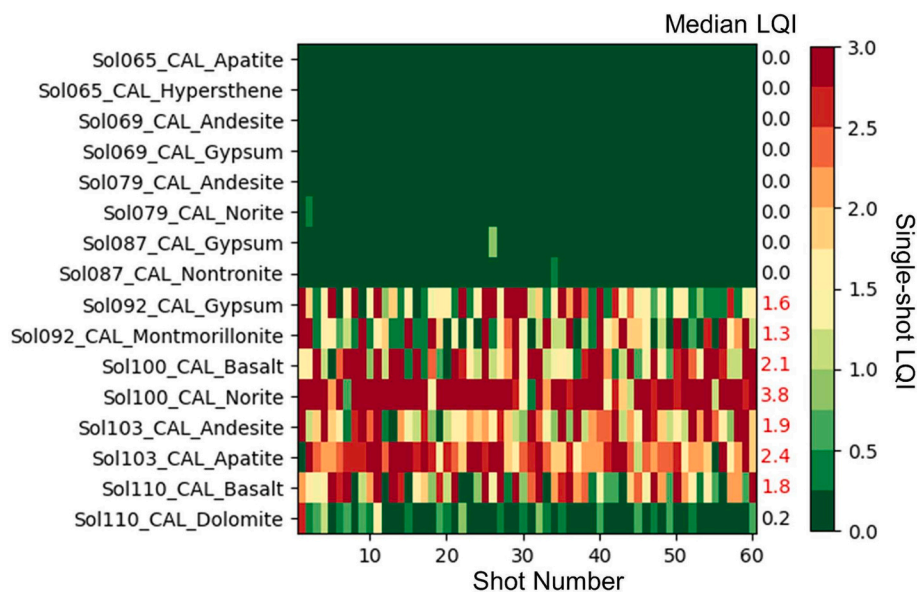


Fig. 8. Single-shot LQI heatmap for onboard calibration target observations from Sol 65–110 by MarSCoDe on Mars. The median LQI for each observation is noted at the right of each row. Median LQI values >1.0 are colored red. (For interpretation of the references to colour in this figure legend, the reader is referred to the web version of this article.)

LQI value between 1 and 3 suggests suspicious data that may have the possibility of focus loss and some deviation in the data similarity with the laboratory dataset. This feature of the LQI eases the data selection process and is sufficient to raise the awareness of data users for certain portions of the data and promote caution in further data filtering and analysis (e.g., applying machine learning).

3.1.4. Applicability of LQI thresholding

The LQI thresholding technique should be applicable to other ChemCam data, as well as to MarSCoDe and SuperCam data, since the LQI calculation followed the same protocol. Here, we present an investigation into the applicability of LQI thresholding beyond the aforementioned Z-stacks, based on the previous knowledge of Mars LIBS data quality.

We first check the LQI thresholding by comparing it with current assessments of potential data quality issues for ChemCam and SuperCam. The PDS data inventories of both instruments contain data comments on target properties, focus issues, data anomalies, etc. [30,39] These comments come from the human inspection during the operation and are based on target images, engineering data (e.g., autofocus profile), spectral characteristics (e.g., total LIBS intensity), quantification results (MOC), etc. There are 150 unique comments for ChemCam and 42 for SuperCam in the Mars data used in this work (see Appendix A.3 and A.4). We first manually organized these comments into 8 different "data tags": AF (potential non-ideal autofocus result), Bad (low total intensity; missed target; night target), Far (long target distance, usually >6 m), Graze (laser pointing at fracture, rough surface, or pebble; high incident angle), Loose (laser pointing at unconsolidated surface), High_MOC (anomaly in total oxide from MOC calibration), High_Ti (significant Ti content), and OK (no comment related to data quality). Graze and Loose "tags" are unique to ChemCam and High_Ti and High_MOC "tags" are unique to SuperCam. If the comment poses multiple issues, the tagging priority will be Bad $>$ Far $>$ AF $>$ Loose/High_Ti $>$ Graze/High_MOC so that each observation has only one "tag". The detailed assignment of these "tags" is listed in Appendix A.4. The distribution of LQI values for each "tag" is shown in Fig. 7.

From the comparison in Fig. 7, it is clear that the observations with manually identified quality issues in their data comments tend to result in higher LQI values. Around 50% of the ChemCam data and 75% of the SuperCam data with no identified issue (OK "tag") lies within LQI $<$ 1

and their major population is within LQI $<$ 3. With LQI ≥ 2 , most of the data with the Bad "tag" for both instruments and data with the Far "tag" for ChemCam can be picked out. The long-distance data with known low total intensities for SuperCam were always tagged Bad first so that the rest Far-tagged data usually have moderate total intensities. Their LQI values were still found to be largely >1 , agreeing with the suspicious nature of the data from targets beyond the normal distance. The Graze and Loose tagged data are related to the concern from the original ChemCam data comments that the surface morphology and consolidation may affect the data quality. These concerns are usually associated with some uncertainty as the exact surface conditions at the natural targets are complicated. As shown in Fig. 7, the LQI result can address this uncertainty by providing a wide range of LQI values for Graze/Loose-tagged data. The detailed effect of material consolidation and morphology on the data quality will be examined in Section 3.3.3.

The High_Ti tagged data with high LQI values are the consequence of Ti's interference on C-658 fit, which will be further discussed in Section 3.1.5. The erroneous MOC seems to be less correlated to data quality from the LQI values of High_MOC tagged data. The relationship between major element quantification and data quality of ChemCam and SuperCam will be investigated later in Section 3.3.4.

To test the applicability of the technique on MarSCoDe, we selected several observations of its onboard calibration targets from Sol 92 to 110 that were previously known to be out of focus. At the start of Zhurong's mission, from Sol 21 to Sol 110, the calibration observations were designed to be focused based on their pre-determined distances to MarSCoDe from pre-flight measurements. But examinations of the data from Sol 92 to 110 revealed lower total intensities, higher shot-by-shot standard deviations, worse C-658 SNR, and significant quantification errors (also partially discussed in Ref. [19]) compared to earlier calibration data. Thus, the predefined distances were presumably shifted during the rover operation and the focus strategy for calibration targets was consequently reprogrammed to rely on the same autofocus mechanism that was used to probe Mars surface targets (defined in Ref. [5] and also discussed in Section 3.3.1).

The shot-by-shot LQI values of these out-of-focus observations were compared with several previous sols without the focus issue, as shown in Fig. 8. The difference in LQI values is significant: the out-of-focus data has LQI $>$ 1 for most of the observations and up to a 60-shot median LQI of 3.8, while well-focused data has achieved LQI values close to 0. One

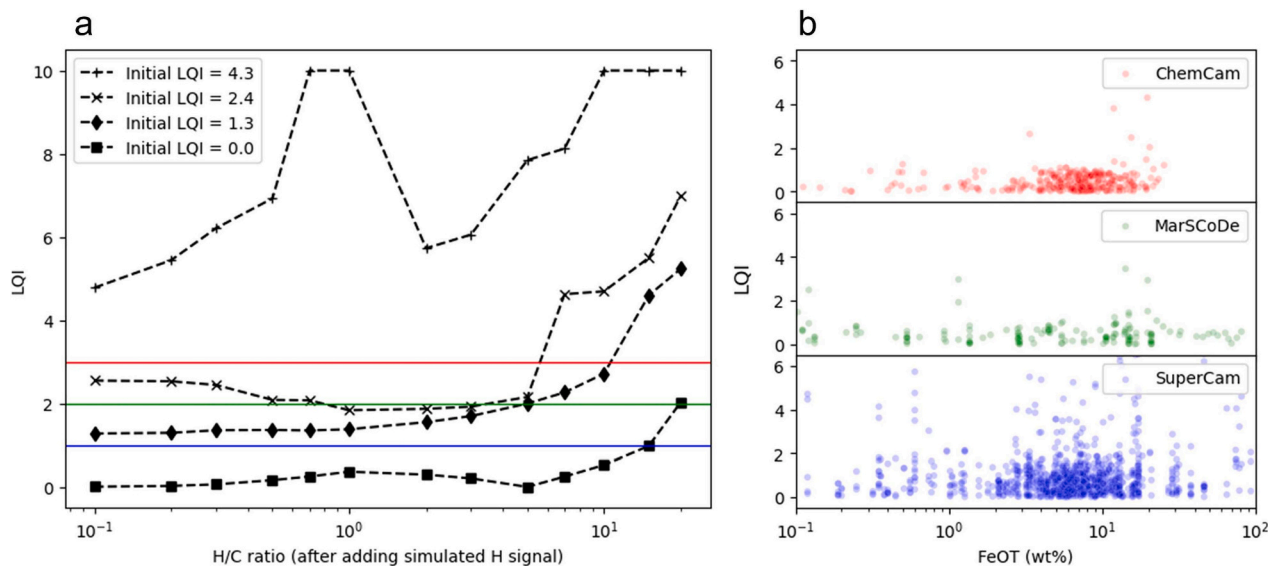


Fig. 9. Robustness tests for LQI against H and Fe emissions. a) LQI values of four selected steps from a ChemCam Season 2 Z-stack (first Z-stack on Mojave_Chunks) upon adding various levels of simulated H signal. LQI = 1,2,3 are marked horizontally. b) LQI values of the laboratory datasets from the three instruments as a function of their certified FeOT contents [16,17,19].

exception is the Sol 110 dolomite target which contains mineralogical carbon. The dolomite observation itself should be also out-of-focus since the first shot on the dust had a high LQI. But later ablations on the dolomite, which excited carbon from the target, scored quite low in LQI values. This additionally signifies the influence of carbonate on the LQI, which could hinder the use of LQI in carbonate-rich targets. Several studies have proposed methods to distinguish carbonate through LIBS spectra (e.g., Refs. [44–46]) and possible laboratory experiments could help determine an upper limit for carbonate concentration before it interferes with LQI. These are subjected to further study.

These investigations demonstrate that the interpretation based on LQI thresholding is generally consistent with the current knowledge of Mars LIBS data quality status that previously relied on human inspection or simple parameters such as the total intensity. Therefore, LQI thresholding is considered to be an applicable and cross-instrument tool for the

evaluation of Martian LIBS data. The possible limitations and interfering factors are discussed in the following section.

3.1.5. Robustness against interference

The concern that the surrounding H_{α} and Fe lines would interfere with the main fit was addressed either by the main fit itself, which fits both H_{α} and C-658 emission, or the Fe treatments mentioned in Section 2.2. The effectiveness and possible limitations of these methods were verified in this section.

First, the effect of different levels of H emission on the LQI values was investigated by introducing a series of additive simulated H signals to the actual LIBS data and calculating the resulting LQI. Four steps with different focus offsets from a ChemCam Season 2 Z-stack (first Z-stack on Mojave_Chunks, same as Fig. 5, with the original H:C peak ratios being around 0.4–0.5 for selected steps) were tested here. The added H lines

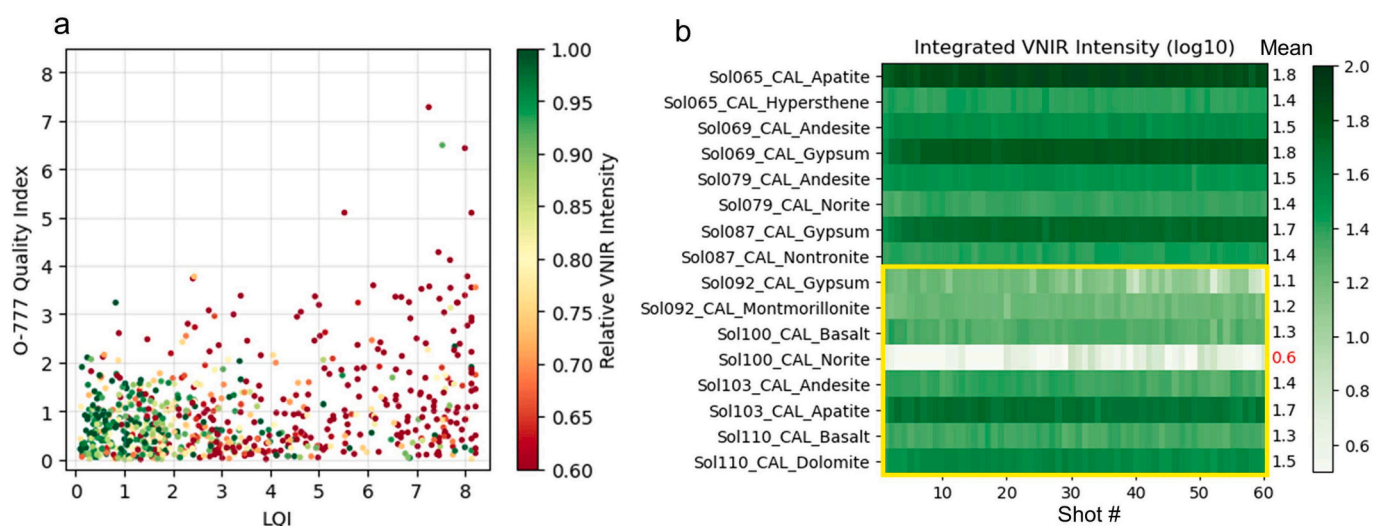


Fig. 10. a) A scatter plot of ChemCam Season 2 Z-stack steps over their LQI values (x-axis), O-777 quality index (y-axis), and relative VNIR intensity (points with intensity below 0.6 were colored the same). b) Shot-by-shot integrated VNIR intensity heatmap for onboard calibration target observations from Sol 65–110 by MarSCoDe on Mars. The intensity unit is originally $W/m^2/sr/nm$ [5]. Common logarithm values are used here for better visualization. The mean integrated VNIR intensity for each observation is noted at the right of each row. Mean values < 1.0 is colored red. (For interpretation of the references to colour in this figure legend, the reader is referred to the web version of this article.)

Table 2

Evaluation of positive and negative predictive values (*PPV* and *NPV*) on task: using the Z-score empirical rule on LQI (filtering the data with LQI < 1,2, or 3) to identify the good focus steps with relative VNIR intensity > 0.8. Both results from median LQI values and single-shot LQI values are shown.

Thresholds	Median LQI		Single LQI	
	<i>PPV</i>	<i>NPV</i>	<i>PPV</i>	<i>NPV</i>
LQI < 1	80%	69%	62%	70%
LQI < 2	73%	80%	61%	79%
LQI < 3	62%	83%	55%	83%

were set to have a uniform Voigt profile with $\sigma_H = 0.37$ (Table 1) and $\gamma_H = 0.52$ (mean values for hydrogen lines from the ChemCam laboratory dataset). The LQI variations against the added H:C peak ratios were tracked in Fig. 9a. It was discovered that an H addition up to 5 times the C-658 peak area could be tolerated by the algorithm: for observations with LQI < 3, the LQI changes < 1 upon the additions; for LQI > 3, H additions didn't induce any categorical change when following the designation in Table 3. The simulation suggests that the H signal may bring uncertainty to the main fit and level the LQI values only at a high relative intensity (H:C ratio > 5), which may affect some dust or hydrated mineral observations whose H:C ratios can go up to 20 (e.g., Ref. [47]).

We then checked the LQI's robustness against the Fe emissions by correlating the LQI values on the laboratory datasets with their FeOT contents, since multiple Fe lines are hard to simulate directly as is the case with the H emission. No significant correlation was found among the three instruments (Fig. 9b), which implies that the surrounding Fe lines have little interference with the LQI method within the given FeOT contents by laboratory datasets. However, the majority of the samples in the laboratory datasets lie within a low-medium FeOT range, e.g., < 20–25%, leaving higher FeOT contents yet to be tested. In practice, there has been no correlation between predicted FeOT content and LQI value for the Mars data (Fig. S4) but an interaction between data quality and FeOT model behavior can't be ruled out.

Another interference may be present by several Titanium emissions in this region as mentioned in Section 3.1.2 and Section 3.1.4, e.g., Ti I 656.743 nm, Ti I 657.700 nm, etc. (all wavelength in vacuum [35]). While no treatment for Ti is presented in this study, LQI values for laboratory datasets also show no significant correlation with TiO₂ contents up to about 3 wt% (Fig. S5). The ChemCam example interfered by Ti peaks as shown in Fig. S3(2) has a modeled TiO₂ of 2.12 ± 0.79 wt%. The High-Ti tagged SuperCam data in Fig. 7 were usually commented to have TiO₂ > 2.4 wt%. Therefore, we could consider an approximate TiO₂ content upper limit for LQI use as 2–3 wt%.

3.2. Comparison with other quality indicators

Oxygen emissions are sometimes considered constant across Mars materials due to the near-constant abundance of oxygen, and oxygen line intensity has been used as a good normalization divisor (e.g., Refs. [15, 47]). Do these properties make Oxygen another indicator of data quality? We applied a similar formulation as LQI to Oxygen triplets around 777 nm (neutral emissions at 777.408, 777.631, and 777.753 nm in vacuum, abbr. O-777) to check if it behaves like C-658-based LQI. The quality index from O-777 was evaluated with ChemCam Season 2 in the same way as described in Section 3.1.2. The LQI and O-777 quality index were plotted together and compared in Fig. 10a. The O-777 quality index shows a clear threshold of about 2, beyond which relative VNIR intensities are low. However, it discriminates the data less effectively below 2, rendering it less sensitive to excitation than LQI (*PPV* and *NPV* for O-777 quality index < 2 are 46% and 90%, respectively, following the same evaluation as Table 2). Oxygen, although approximately constant in most of the targets, is partially excited directly from the target by the laser, unlike the atmospheric carbon, which is likely to give a different

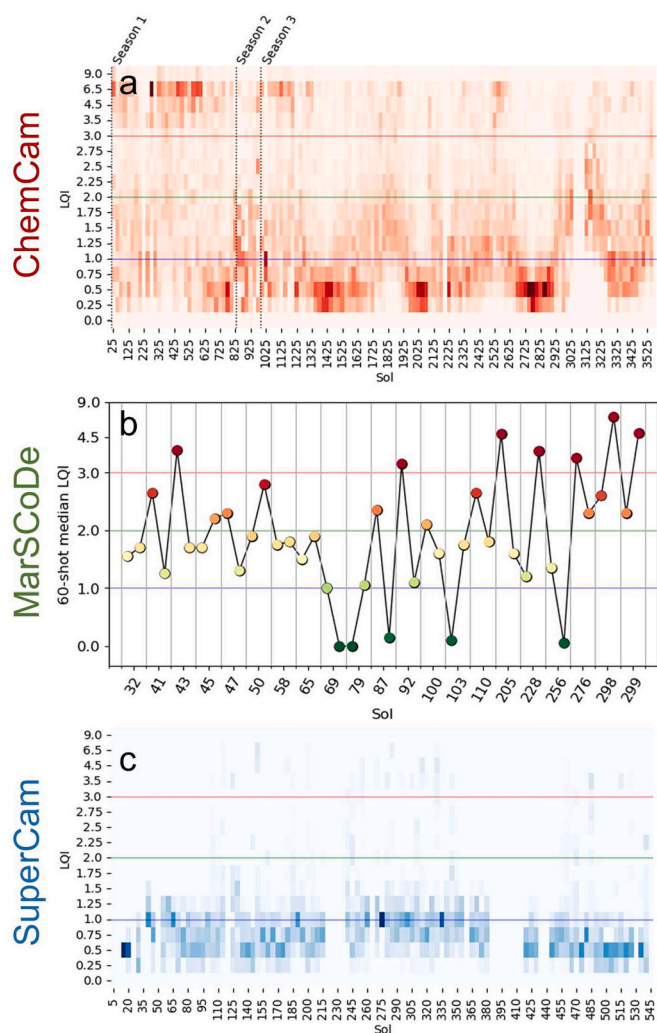


Fig. 11. Synthesis of LQI results on the three Martian LIBS instruments (ChemCam, MarSCOde, and SuperCam). Calibration data were not included. For all panels, LQI = 1,2,3 are marked with horizontal lines corresponding to Table 3. The LQI axis is linearly scaled for LQI < 3, beyond which a square-root scale is applied to plot a wider LQI range. a) ChemCam data distribution based on target LQI values with operation sols. The sols are binned in a 25-sol interval and the distribution is normalized per sol interval for better visualization, i.e., each pixel value represents the data percentage among the data in the same sol interval, and the darker the colour, the greater the value. Beginnings of operational seasons are marked with vertical dotted lines (Season 2 @ Sol 801, Season 3 @ Sol 983). b) MarSCOde target LQI values along all sols with LIBS operation. Each sol always contains two targets. c) SuperCam data distribution based on target LQI values with sols. The sols are binned in a 5-sol interval. The normalization is the same as the panel a).

reaction of the O-777 quality index to the input irradiance. This result emphasizes the philosophy behind a good quality index, that not only a constant presence is required, but also a theoretical and practical sensitivity to the input irradiance is necessary.

Another common quality indicator is the total VNIR intensity of the spectrum. However, it can be fuzzy when setting thresholds for the fine evaluation of quality beyond picking outliers. The same MarSCOde examples shown in Section 3.1.4 were also evaluated by shot-by-shot and averaged integrated VNIR intensity (Fig. 10b, VNIR range for MarSCOde is defined from 540 nm to 850 nm). We found that the boundary between the good data (Sol 65–87) and out-of-focus data (Sol 92–110) cannot be clearly defined by simply thresholding the integrated VNIR intensity. Furthermore, there is a significant scatter of VNIR intensities among the good data. This property makes the VNIR intensity as a less

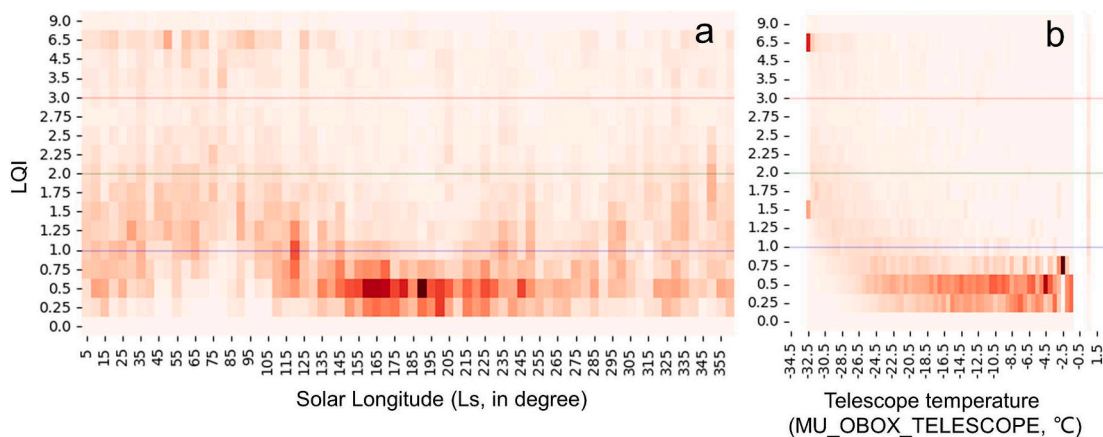


Fig. 12. a) Distribution of ChemCam data based on LQI values with solar longitude (Ls). The Ls span is binned in a 5-degree interval. b) Distribution of ChemCam data based on LQI values with the MU_OBOX_TELESCOPE parameter in ChemCam LIBS data headers. The temperature is binned by 0.5-degree intervals and the distribution is normalized per temperature interval for better visualization. For all panels, LQI = 1,2,3 are marked horizontally.

refined quality indicator than LQI.

3.3. LQI applications on Martian LIBS data

With the LQI technique, we evaluated the data quality of the LIBS spectra from the three Martian LIBS instruments, ChemCam (Sol 10–3546), MarSCoDe (Sol 32–299), and SuperCam (Sol 12–538) in Fig. 11. The LQI value for each individual shot was calculated, from which a median LQI was generated for each target, namely the target LQI value. The discussion below focuses on demonstrating LQI's capability and the insights that the LQI can provide from the focus strategy, environmental conditions, target properties, and elemental quantification.

3.3.1. Autofocus (AF) strategy

Several AF strategies have been utilized on Mars by current LIBS instruments. Continuous wavelength laser (CWL) AF technique is implemented on all three Martian LIBS instruments [1,3,5]. This active AF technique utilizes the reflected CWL intensity to determine the best focus, which is less affected by environmental illumination or target texture [3]. However, ChemCam's CWL failed in 2014, 2.3 years into the mission [28], which led to the development of Remote Micro-Imager (RMI) AF. The RMI technique is passive and image-based, relying on the target's illumination and sharpness to focus, but its searching for the best focus is thought to be finer than CWL in certain cases and can focus with no distance limit [3]. RMI AF is now used by ChemCam and SuperCam as the primary technique [3,28]. Both techniques above require a correction from their best focus to the best laser focus. LIBS AF searches the best focus directly using a series of LIBS intensity feedback, which has been previously tried on ChemCam during Season 2 [28] and also implemented in MarSCoDe as the fine-focusing mechanism guided by CWL [5]. Also, focusing laser with the LIBS acoustic signal [48] can be considered as a kind of LIBS AF.

Through the LQI evaluation, we discovered that these AF techniques (and their combinations) may not perform equally well in reproducing an optimal excitation, as shown in Table 4. ChemCam achieved better LQI in Season 3 than in Season 1 after employing the RMI AF. SuperCam's RMI AF performed very well with 94% of target LQI values lying within LQI < 2. Meanwhile, MarSCoDe's CWL + LIBS AF scored similarly to early ChemCam's CWL AF while the result carries some uncertainty due to the data being limited in number. The limitation of LIBS AF is that the technique disturbs the target prior to the main observation and may ablate off some material that should have been at the best focus position, which is expected to affect the method on some unconsolidated targets [19]. The influence of target material is discussed further in

Section 3.3.3. The result here suggests that RMI AF is a better technique to achieve optimal excitation on Mars compared to other implemented techniques.

3.3.2. Environmental condition

From Fig. 11a, we also discovered a seasonal oscillation in the data distribution for ChemCam Season 3. This phenomenon is further clarified in Fig. 12a by plotting the distribution as a function of solar longitude (L_s). A similar oscillation of the carbon-oxygen line ratio has also been discovered by Beck et al. [46]. Many correlations were found in this seasonal phenomenon, e.g., between LQI values and atmospheric pressure (Fig. S6b), and between LQI values and ChemCam Mast-unit (MU) optical box (OBOX) temperature (the MU_OBOX_TELESCOPE parameter in ChemCam LIBS data headers), as shown in Fig. 12b and Fig. S6a. These may indicate that some seasonal conditions may have influenced the data quality.

The strong correlation between LQI and MU_OBOX_TELESCOPE may explain the seasonal oscillation better than involving atmospheric pressure since the positive correlation with pressure (Fig. S6b) contradicts Eq. 10 which implies that a high $p(\text{CO}_2)$ enhances C-658 emission. This correlation with pressure may be only coincidental due to the weak co-variation of the pressure and MU_OBOX_TELESCOPE (Fig. S6c). The influence of MU_OBOX_TELESCOPE on the data quality may be related to instrumental aspects such as the wavelength calibration or the AF mechanism.

The temperature-variable wavelength calibration may affect the line width of C-658. However, this effect should be present in all targets, including calibration targets, whose LQI values do not show significant seasonal changes (Fig. S6d).

The offset between the RMI AF focus and the exact LIBS focus could play a role in this phenomenon. The offset is temperature dependent and both ChemCam and SuperCam rely on calibration to facilitate the RMI AF at varying temperatures [3]. However, no significant seasonal variation was observed for SuperCam (Fig. S6e). A key difference between ChemCam and SuperCam is that the ChemCam RMI AF was remotely experimented and calibrated on Mars and only for a small part of a Martian year. The offset-temperature calibration established during this period has a limited OBOX temperature coverage from -29.8 to -7.5 °C, according to Season 2 data on PDS, but the exact temperatures of OBOX could be as low as -32.7 °C throughout the whole year. The possibly inadequate calibration of the ChemCam may have contributed to the seasonal inaccuracy of the ChemCam RMI AF. While identifying a definite cause for the problem is beyond the scope of this study, this investigation of the environmental condition by LQI evaluation demonstrates the technique's sensitivity and its diagnostic potential for

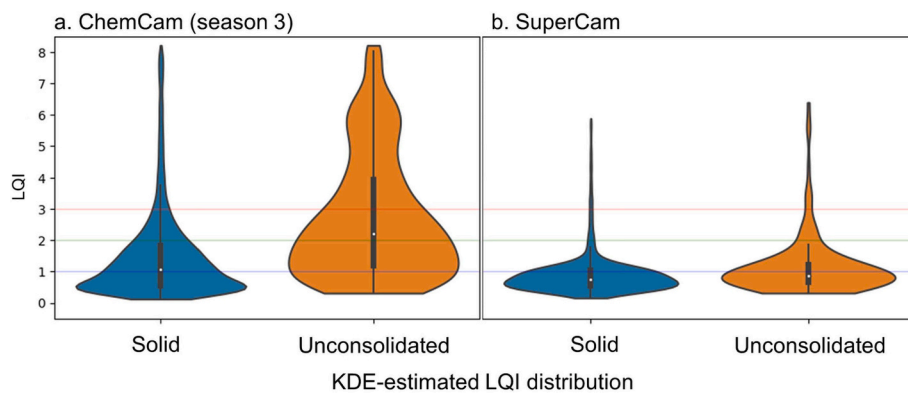


Fig. 13. Violin plots for LQI distributions between solid (rock, bedrock, vein in the master lists) and unconsolidated (regolith, dune, pile, sand in the master lists) target types [30,39] for a) ChemCam Season 3 and b) SuperCam. The median LQI values of the targets were used. The KDE methodology is the same as Fig. 2. For all panels, LQI = 1,2,3 are marked horizontally.

Martian LIBS instruments.

3.3.3. Material consolidation and morphology

The influence of material consolidation on plasma excitation was also investigated by LQI. For both ChemCam and SuperCam, targets identified as unconsolidated (including anything recorded as regolith, dune, pile, sand, etc., in the master lists) scored relatively higher LQI values than targets identified as solid (rock, bedrock, vein in the master lists [30,39]), while for SuperCam the difference is visually smaller than for ChemCam (Fig. 13, differences in median LQI between rock and soil subsets were 1.15 and 0.12 for ChemCam and SuperCam, respectively).

The influence of consolidation may originate from the laboratory datasets on which the LQI evaluation was built, which typically contain only consolidated ceramic, glass, or pellet targets (e.g., Refs. [19, 49–51]). This determined that the excitation could be different for unconsolidated targets. Also, the line broadening may also have been affected by the consolidation [41]. The reason why SuperCam is less affected than ChemCam may be related to the higher irradiance: at 3 m, the intensity is greater than 6 GW/cm² for SuperCam compared to

around 3 GW/cm² for ChemCam [1,3], given a general excitation threshold for solids around 1 GW/cm² [1]. We believe that an expanded database with unconsolidated material (and even a dedicated LQI established on powder standards) could be beneficial for a better understanding of data quality, as well as a better quantification by LIBS.

The morphology of the material surface can also influence the data quality of LIBS spectra, as demonstrated in the previous section (Section 3.1.4) by the wide range of LQI values from the data that were produced on fractured, rough, or pebbly surfaces (Graze-tagged data in Fig. 7). Two factors may be involved: the surface roughness and the ablation angle. The surface roughness at mm-scale is known to influence the hydrogen signal [52]. The increase of the exposed surface in contact with the LIBS plasma may supply an additional hydrogen signal to strengthen the H_α emission [52], potentially levelling the H:C ratio beyond the tolerance mentioned in Section 3.1.5. Meanwhile, the roughness at sub-laser spot scales may also act like the porosity in the unconsolidated material, affecting the total amount of material ablated. These can collectively cause the observation on a target appearing to have a rough surface to score a higher LQI.

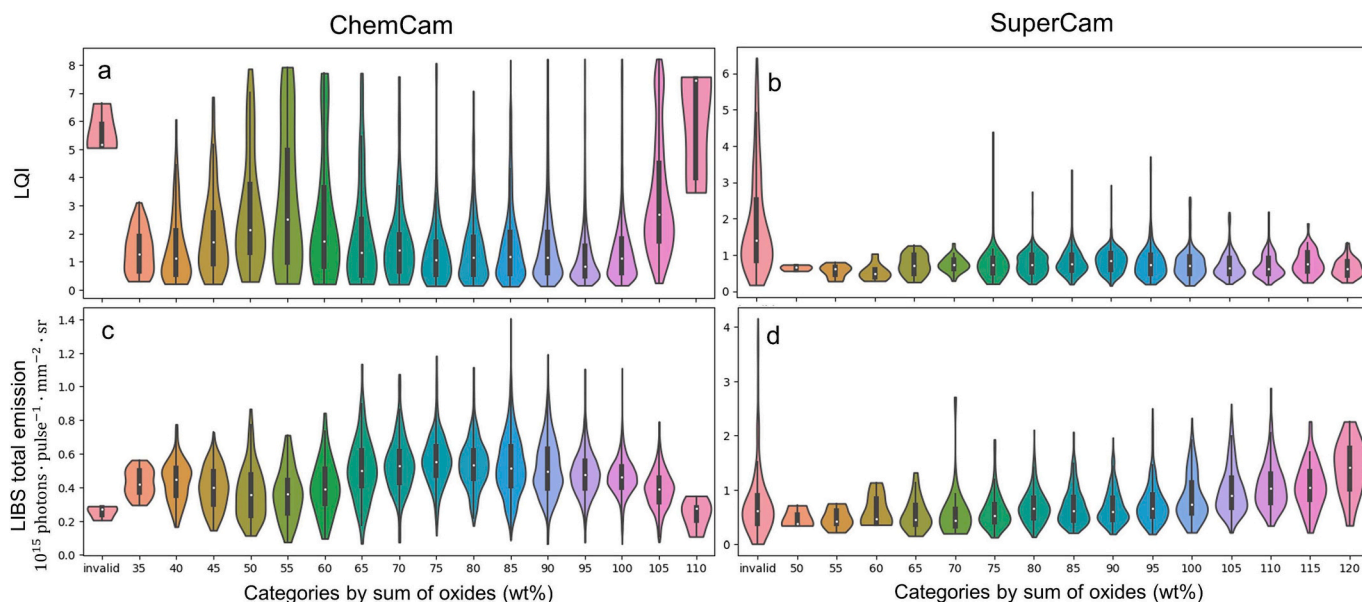


Fig. 14. Distributions of quality statistics (LQI or LIBS total emission) of Martian LIBS data categorized by their MOC-predicted sum of oxide contents (including SiO₂, TiO₂, Al₂O₃, FeO, MgO, CaO, Na₂O, and K₂O). The distributions are illustrated in a series of violin plots estimated by the same KDE methodology as Fig. 2. The LIBS data in each violin are filtered according to their sum of oxides values which are within a 5 wt% interval centered at the value annotated on the corresponding x-axis category. The "invalid" category represents the data whose MOC are not present on the PDS. The quality statistic and the instrument for each panel: a) LQI of ChemCam data; b) LQI of SuperCam data; c) LIBS total emission of ChemCam data; d) LIBS total emission of SuperCam data.

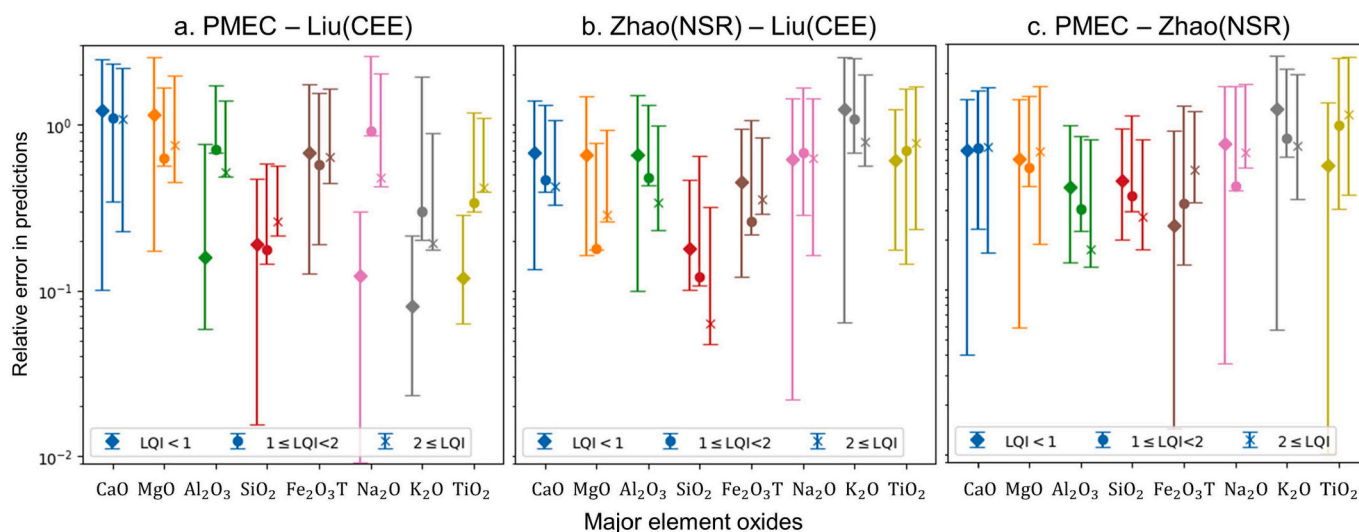


Fig. 15. Inconsistency between selected models as a function of oxide types (by major x-axis offsets and colors) and LQI ranges (by minor x-axis offsets and markers). The relative error is defined as the absolute error between two predictions divided by their mean. The marker position represents the median of relative errors. The error bars indicate the min-max relative error ranges.

Surface roughness or specific morphology may cause the laser to ablate the target at a high incident angle. Previous studies have reported a decrease in total LIBS intensity for incident angles $>50^{\circ}$ – 60° [53–55]. The systematic investigation by Breves et al. [56] has also suggested the significantly lower laser irradiance at a high ablation angle, which could affect the irradiance-sensitive C-658 emission. The LQI distribution of the ChemCam data tagged Graze in Fig. 7 agrees with this statement. Among these data tagged, for example, ten observations on consolidated target Barto_Lake were clearly commented with high ablation angles and resulted in a median LQI value of 1.8, and seven of them scored LQI > 1 . A systematic investigation of the Mars target images, LQI values, and other data quality metrics could help to determine the optimal surface morphology for LIBS observations on Mars, which would be a worthy topic for future study.

3.3.4. Major elements quantification

3.3.4.1. Major Oxide Composition (MOC) for ChemCam and SuperCam. We checked what information the LQI evaluation could provide for the Major Oxide Composition (MOC) of both ChemCam [16] and SuperCam [17]. As LQI is also an assessment of the data similarity compared to the laboratory dataset, significant quantification errors are expected to correlate with high LQI values. From Fig. 14a, high sums of oxides

(>100 wt%) correlate well with high LQI values, signifying an influence of data quality on the quantification results. However, this was not observed for SuperCam (Fig. 14b), suggesting possible problems other than data quality. This anomaly was further explored by checking Fig. 14cd, where SuperCam data with a high sum of oxides, unlike ChemCam, actually corresponded to higher total emissions than other data. This suggests that there are other factors for erroneous SuperCam MOC results, such as the behaviors of the underlying algorithms between ChemCam (PLS + ICA) and SuperCam (ensemble learning) towards their specific local materials. This analysis showed that the erroneous quantification for LIBS spectra could be analyzed and attributed distinguishably to the data quality or the other factor using LQI as a figure of merit for data quality.

3.3.4.2. Quantification for MarSCOde. MarSCOde carried by China's first Mars rover Zhurong marked a new frontier for the LIBS operation in Utopia Planitia. Many quantification attempts have been made for the MarSCOde LIBS to better understand the local chemistry, which presents an opportunity to study how LIBS data quality influences the results of different models. Here, we have selected three studies with three different quantification methodologies summarized in Table 5 and tried to examine how the inconsistency among their results on Martian targets evolved with the data quality.

Table 3

Proposed LQI thresholds, intervals, and their interpretations for data similarity, focus quality, spectral quality, etc. The factors that may cause outlier situations, i.e., possible issues with LQI robustness, are further discussed in Section 3.1.5.

LQI range	0	1	2	3	inf
Quality Evaluation	Good		Moderate	Cautious	Outlier
Excitation	Well-excited		Intermediate excitation		Insufficient excitation with high confidence
Similarity	Excitation similar to at least ~68% of the laboratory dataset, good for applying machine learning models.		Excitation is deviated from at least ~68% of the laboratory dataset, apply machine learning with caution.	Excitation similar to at most ~5% of the laboratory dataset; machine learning may produce higher uncertainty.	Excitation deviated from the laboratory dataset; not suitable for applying machine learning.
Other comment	Optimal excitation/focus		Distorted line ratios may appear; possible suboptimal focus, or target beyond usual distance; possible interference*.		Possibly strong interference*, poor focus, or far target

* Interference by Fe, H, or Ti to the C-658 fit.

Table 4

Target LQI value distributions for Martian LIBS instruments with different AF strategies.

Instrument	AF strategy	LQI < 1	1 ≤ LQI < 2	2 ≤ LQI < 3	LQI ≥ 3
ChemCam	CWL (before sol 801)	33%	21%	14%	32%
	RMI (after sol 983)	48%	25%	13%	14%
MarSCoDe	CWL + LIBS	26%	31%	21%	22%
SuperCam	Mostly RMI	65%	29%	3%	3%

Here, the inconsistency between any two particular models was measured by the relative errors between their predictions, as shown and explained in Fig. 15. Inconsistencies were found to increase with LQI values for certain occasions. Examples of high inconsistency gains upon low quality include the Al₂O₃, SiO₂, Na₂O, K₂O models between P MEC and Liu(CEE), Na₂O, K₂O models between Zhao(NSR) and Liu(CEE), and Fe₂O₃T, Na₂O, K₂O models between P MEC and Zhao(NSR).

The inconsistency between models could be attributed to two factors: 1) systematic bias caused by the model architectures themselves; and 2) uncertainty brought by the low data quality. Similar to the previous section, these factors can be distinguished in this investigation using the LQI assessment of data quality. From the comparison in Fig. 15, Na₂O and K₂O inconsistencies were considered to be dominated by the data quality. The explanation may relate to the methodologies for Na, K predictions that focus only on certain emissions: Na I 589.2 and K I 766.7 carried high prediction importance in P MEC [19] and were both used by Zhao(NSR) [57] and Liu(CEE) [24], leading to less inter-model systematic bias. On the other hand, the systematic bias can overwhelm the inconsistency due to data quality when the model architectures are very different, e.g., the univariate Zhao(NSR) models versus the more complicated Liu(CEE) and P MEC models.

4. Conclusions

The LIBS Quality Index (LQI) developed in this paper is an evaluation of the plasma excitation for Martian in-situ LIBS spectra. The LQI evaluation uses the sensitive and atmospheric emissions of the C II doublet around 658 nm (C-658) as an indicator of the input irradiance and therefore the plasma excitation to form a Z-score-like index that describes: 1) the signal-to-noise ratio of the emission and 2) the consistency of the Lorentzian width of the emission compared to those from laboratory datasets, based on the fact that the Lorentzian width values in laboratory datasets are found to be unimodal.

The methodology practically includes 1) a main multi-Voigt fit involving both C-658 and neighboring H_α emission; 2) treatments of the surrounding Fe emissions to reduce their interference on the results; 3) noise-adding bootstrapping of the main fit to produce stable statistics for fitted parameters. Uncertainty in the evaluation can be further reduced by using the median LQI from single-shot LQI values within a given observation.

The LQI routine for each instrument was established with

Table 5

Selected quantification models to compare in this study. Except for the probabilistic major element composition (P MEC) by Ref. [19], model nomenclatures are formatted in First Author(Journal abbreviation) for the ease of discussion: Liu(CEE) from Ref. [24] and Zhao(NSR) from Ref. [57].

Model	Algorithms	Training Detail	Number of Features	Normalization
P MEC [19]	NGBoost	Models were trained with 93 standards measured by the MarSCoDe flight model.	full spectrum (245–845 nm)	Integrated intensity of full spectrum (Norm1)
Liu(CEE) [24]	Transferred multivariable polynomial	Models were trained with spectra of 295 samples measured by ChemCam replica [16] and transferred to MarSCoDe using shared Norite calibration targets.	14 selected lines	Sum intensity of 14 lines
Zhao(NSR) [57]	Univariable	Models were fitted with 4 MarSCoDe Norite observations on Mars.	1 line for each oxide	C I 247.9 nm

instrument-specific parameters and laboratory dataset. Its Z-score-like formulation allows the use of a general 1,2,3-sigma rule and provides the interpretations of the LQI as 1) a confidence level for "poor" excitation and 2) a measure for similarity to the laboratory dataset, as proposed in Table 3. These interpretations were justified with the laboratory datasets from ChemCam, MarSCoDe, and SuperCam, the Z-stack data from ChemCam Season 2 focus experiments, ChemCam and SuperCam data from Mars with manually commented quality issues, and the known out-of-focus calibration data from MarSCoDe on Mars. The methodology also outperformed other possible indicators such as the oxygen emissions around 777 nm and the total VNIR intensities in assessing the data quality.

Certain limitations were posed for the methodology: 1) LQI is not compatible with carbonate targets; 2) interference from other emissions could compromise the evaluation under certain conditions such as high hydrogen (H:C peak ratio > 5), possibly high Fe (FeOT over 20–25 wt%), or high Ti (TiO₂ over 2–3 wt%) materials; 3) single-shot LQI values still carry some uncertainty in identifying the well-excited data. The boundaries/conditions for these limitations are well-defined so that suspicious LQI values can be treated with caution.

With the LQI in hand, we evaluated the data quality of the Martian LIBS spectra from ChemCam, MarSCoDe, and SuperCam. Several discoveries were made with the index:

1. ChemCam data quality has improved following the reworking of the autofocus strategy after the CWL failure. Currently, the in-operation RMI AF of ChemCam and SuperCam outperforms the previous CWL AF and CWL + LIBS AF as indicated by their data LQI values. The result suggests that RMI AF is a better AF mechanism for in-situ operation on Mars.
2. For the RMI AF of ChemCam in its Season 3 operation, a seasonal variation in data quality was discovered, which may be related to the temperature calibration on the offset between RMI focus and LIBS focus.
3. Target consolidation and morphology can affect the data quality. Data on solid targets are better-excited than those on unconsolidated targets. Surface roughness and the laser ablation angle can also influence the data quality.
4. Both model behavior and data quality could contribute to the prediction uncertainty and the inconsistency among multiple methodologies of the major element quantification from LIBS spectra.

These application examples demonstrate the feasibility of the LQI as a useful and sensitive tool to evaluate data quality and its potential to select the optimal instrumental design, to assist the operational decision, and to investigate the quantification uncertainty. We believe that this well-quantified and excitation-related data quality index will help to reveal the focus effect of Martian in-situ LIBS in future works: How does the plasma excitation affect the spectra? What kind of normalization should we implement to unify observations of various excitations, not only for each individual instrument but also for all Martian LIBS alike?

CRedit authorship contribution statement

Zhaopeng Chen: Conceptualization, Methodology, Software, Validation, Investigation, Data curation, Formal analysis, Writing – original draft, Writing – review & editing, Visualization, Funding acquisition. **Olivier Forni:** Conceptualization, Methodology, Validation, Data curation, Writing – review & editing, Supervision. **Agnès Cousin:** Conceptualization, Methodology, Resources, Writing – review & editing, Supervision, Project administration. **Paolo Pilleri:** Software, Validation, Data curation, Writing – review & editing. **Olivier Gasnault:** Resources, Writing – review & editing. **Sylvestre Maurice:** Conceptualization, Writing – review & editing, Resources, Project administration, Supervision, Funding acquisition. **Roger C. Wiens:** Conceptualization, Writing – review & editing, Resources, Project administration. **Yizhong Zhang:** Data curation. **Yuxuan Luo:** Data curation. **Xin Ren:** Conceptualization, Resources, Supervision. **Weiming Xu:** Resources, Data curation. **Xiangfeng Liu:** Software, Resources, Data curation. **Rong Shu:** Supervision, Project administration. **Chunlai Li:** Resources, Supervision, Writing – review & editing, Funding acquisition.

Declaration of competing interest

The authors declare that they have no known competing financial interests or personal relationships that could have appeared to influence the work reported in this paper.

Data availability

Data will be made available on request.

Acknowledgements

This study was funded by Centre National d'Etudes Spatiales (CNES, France), the Key Research Program of the Chinese Academy of Sciences (Grant No. ZDBS-SSW-TLC001), and the China Scholarship Council (for the joint Ph.D. program of Z. Chen, No. 202204910345). We are especially grateful to Dr. Pierre Beck for the beneficial discussion on carbon lines in LIBS plasma. We are grateful to the colleagues from the Key Laboratory of Lunar and Deep Space Exploration, NAOC who provided data curation support for MarSCODe. We thank the journal editorial team for handling the manuscript and thank the two anonymous reviewers for their insightful suggestions to improve the manuscript.

Appendix A. Supplementary data

Supplementary data to this article can be found online at <https://doi.org/10.1016/j.sab.2024.106921>.

References

- S. Maurice, R. Wiens, M. Saccoccio, B. Barraclough, O. Gasnault, O. Forni, N. Mangold, D. Baratoux, S. Bender, G. Berger, et al., The ChemCam instrument suite on the Mars Science Laboratory (MSL) rover: science objectives and mast unit description, *Space Sci. Rev.* 170 (2012) 95–166.
- R.C. Wiens, S. Maurice, B. Barraclough, M. Saccoccio, W.C. Barkley, J.F. Bell, S. Bender, J. Bernardin, D. Blaney, J. Blank, et al., The ChemCam instrument suite on the Mars Science Laboratory (MSL) rover: body unit and combined system tests, *Space Sci. Rev.* 170 (2012) 167–227.
- S. Maurice, R.C. Wiens, P. Bernardi, P. Caïs, S. Robinson, T. Nelson, O. Gasnault, J.-M. Reess, M. Deleuze, F. Rull, et al., The SuperCam instrument suite on the Mars 2020 rover: science objectives and mast-unit description, *Space Sci. Rev.* 217 (2021) 1–108.
- R.C. Wiens, S. Maurice, S.H. Robinson, A.E. Nelson, P. Cais, P. Bernardi, R. T. Newell, S. Clegg, S.K. Sharma, S. Storms, et al., The SuperCam instrument suite on the NASA Mars 2020 rover: body unit and combined system tests, *Space Sci. Rev.* 217 (2021) 1–87.
- W. Xu, X. Liu, Z. Yan, L. Li, Z. Zhang, Y. Kuang, H. Jiang, H. Yu, F. Yang, C. Liu, et al., The MarSCOde instrument suite on the Mars rover of China's Tianwen-1 mission, *Space Sci. Rev.* 217 (2021) 1–58.
- R. Francis, T. Estlin, G. Doran, S. Johnstone, D. Gaines, V. Verma, M. Burl, J. Frydenvang, S. Montañó, R.C. Wiens, et al., AEGIS autonomous targeting for ChemCam on Mars Science Laboratory: deployment and results of initial science team use, *Sci. Robot.* 2 (7) (2017) eaan4582.
- P.-Y. Meslin, O. Gasnault, O. Forni, S. Schröder, A. Cousin, G. Berger, S. Clegg, J. Lasue, S. Maurice, V. Sautter, et al., Soil diversity and hydration as observed by ChemCam at Gale crater, Mars, *Science* 341 (6153) (2013) 1238670.
- X. Qin, X. Ren, X. Wang, J. Liu, H. Wu, X. Zeng, Y. Sun, Z. Chen, S. Zhang, Y. Zhang, et al., Modern water at low latitudes on Mars: potential evidence from dune surfaces, *Sci. Adv.* 9 (17) (2023) eadd8868.
- S. Musazzi, U. Perini, *Laser-induced breakdown spectroscopy*, Springer Ser. Opt. Sci. 182 (2014).
- D.A. Cremers, L.J. Radziemski, *Handbook of Laser-Induced Breakdown Spectroscopy*, John Wiley & Sons, 2013.
- J. Vrengor, R. Noll, V. Sturm, Investigation of matrix effects in laser-induced breakdown spectroscopy plasmas of high-alloy steel for matrix and minor elements, *Spectrochim. Acta B At. Spectrosc.* 60 (7–8) (2005) 1083–1091.
- B. Sallé, J.-L. Lacour, P. Mauchien, P. Fichet, S. Maurice, G. Manhès, Comparative study of different methodologies for quantitative rock analysis by laser-induced breakdown spectroscopy in a simulated martian atmosphere, *Spectrochim. Acta B At. Spectrosc.* 61 (3) (2006) 301–313, <https://doi.org/10.1016/j.sab.2006.02.003>. URL, <https://www.sciencedirect.com/science/article/pii/S0584854706000322>.
- K.H. Lepore, C.I. Fassett, E.A. Breves, S. Byrne, S. Giguere, T. Boucher, J. M. Rhodes, M. Vollinger, C.H. Anderson, R.W. Murray, et al., Matrix effects in quantitative analysis of laser-induced breakdown spectroscopy (LIBS) of rock powders doped with Cr, Mn, Ni, Zn, and Co, *Appl. Spectrosc.* 71 (4) (2017) 600–626.
- R. Wiens, S. Maurice, J. Lasue, O. Forni, R. Anderson, S. Clegg, S. Bender, D. Blaney, B. Barraclough, A. Cousin, et al., Pre-flight calibration and initial data processing for the chemcam laser-induced breakdown spectroscopy instrument on the Mars Science Laboratory rover, *Spectrochim. Acta B At. Spectrosc.* 82 (2013) 1–27.
- S.M. Clegg, R.C. Wiens, R. Anderson, O. Forni, J. Frydenvang, J. Lasue, A. Cousin, V. Payre, T. Boucher, M.D. Dyar, et al., Recalibration of the Mars Science Laboratory ChemCam instrument with an expanded geochemical database, *Spectrochim. Acta B At. Spectrosc.* 129 (2017) 64–85.
- R.B. Anderson, O. Forni, A. Cousin, R.C. Wiens, S.M. Clegg, J. Frydenvang, T. S. Gabriel, A. Ollila, S. Schröder, O. Beyssac, et al., Post-landing major element quantification using supercam laser induced breakdown spectroscopy, *Spectrochim. Acta B At. Spectrosc.* 188 (2022) 106347.
- T. Duan, A. Anand, D.Y. Ding, K.K. Thai, S. Basu, A. Ng, A. Schuler, Ngboost: Natural gradient boosting for probabilistic prediction, in: *International Conference on Machine Learning*, PMLR, 2020, pp. 2690–2700.
- Z. Chen, X. Ren, J. Liu, W. Xu, Y. Zhang, X. Liu, Q. Zhou, W. Chen, Probabilistic multivariable calibration for major elements analysis of Marscode martian laser-induced breakdown spectroscopy instrument on Zhurong rover, *Spectrochim. Acta B At. Spectrosc.* 197 (2022) 106529.
- S.M. Clegg, E. Sklute, M.D. Dyar, J.E. Barefield, R.C. Wiens, Multivariate analysis of remote laser-induced breakdown spectroscopy spectra using partial least squares, principal component analysis, and related techniques, *Spectrochim. Acta B At. Spectrosc.* 64 (1) (2009) 79–88.
- C. Sun, W. Xu, Y. Tan, Y. Zhang, Z. Yue, L. Zou, S. Shabbir, M. Wu, F. Chen, J. Yu, From machine learning to transfer learning in laser-induced breakdown spectroscopy analysis of rocks for Mars exploration, *Sci. Rep.* 11 (1) (Nov. 2021), <https://doi.org/10.1038/s41598-021-00647-2>.
- S. Shabbir, W. Xu, Y. Zhang, C. Sun, Z. Yue, L. Zou, F. Chen, J. Yu, Machine learning and transfer learning for correction of the chemical and physical matrix effects in the determination of alkali and alkaline earth metals with LIBS in rocks, *Spectrochim. Acta B At. Spectrosc.* 194 (2022) 106478, <https://doi.org/10.1016/j.sab.2022.106478>.
- C. Liu, Z. Ling, Z. Wu, J. Zhang, J. Chen, X. Fu, L. Qiao, P. Liu, B. Li, L. Zhang, et al., Aqueous alteration of the vastitas borealis formation at the Tianwen-1 landing site, *Commun. Earth Environ.* 3 (1) (2022) 280.
- E. Képes, J. Vrabel, P. Porížka, J. Kaiser, Improving laser-induced breakdown spectroscopy regression models via transfer learning, *J. Anal. At. Spectrom.* 37 (9) (2022) 1883–1893, <https://doi.org/10.1039/d2ja00180b>.
- J.-B. Sirven, B. Bousquet, L. Canioni, L. Sarger, Laser-induced breakdown spectroscopy of composite samples: comparison of advanced chemometrics methods, *Anal. Chem.* 78 (5) (2006) 1462–1469.
- J.D. Kelleher, B. Mac Namee, A. D'Arcy, *Fundamentals of Machine Learning for Predictive Data Analytics: Algorithms, Worked Examples, and Case Studies*, MIT Press, 2020.
- L. Peret, O. Gasnault, R. Dingler, Y. Langevin, S. Bender, D. Blaney, S. Clegg, C. Clewans, D. Delapp, C.M. Donny, et al., Restoration of the autofocus capability of the ChemCam instrument onboard the Curiosity rover, in: *14th International Conference on Space Operations*, 2016, p. 2539.
- H. Manelski, R. Wiens, S. Schroder, P. Hansen, B. Bousquet, B. Martin, S. Clegg, LIBS plasma diagnostics with supercam on Mars, *LPI Contrib.* (2024) 1570.
- Mars 2020 Supercam Masterlist. https://pds-geosciences.wustl.edu/m2020/urn-na-sa-pds-mars2020_supercam/data_observation_log/m2020_scam_masterlist.csv, 2023.
- Z. Chen, S. Maurice, F. Olivier, A. Cousin, P. Pilleri, Y. Zhang, Y. Luo, X. Ren, C. Li, W. Xu, X. Liu, R. Shu, A quality index for martian in-situ LIBS spectra, *LPI Contrib.* 2806 (2023) 1480.
- J.L. Bandfield, T.D. Glotch, P.R. Christensen, Spectroscopic identification of carbonate minerals in the martian dust, *Science* 301 (5636) (2003) 1084–1087.
- J.-P. Bibring, Y. Langevin, J.F. Mustard, F. Poulet, R. Arvidson, A. Gendrin, B. Gondet, N. Mangold, P. Pinet, F. Forget, et al., Global mineralogical and aqueous

- mars history derived from omega/mars express data, *Science* 312 (5772) (2006) 400–404.
- [34] W.M. Haynes, *CRC Handbook of Chemistry and Physics*, CRC Press, 2016.
- [35] A. Kramida, Yu. Ralchenko, J. Reader, and NIST ASD Team, *NIST Atomic Spectra Database* (ver. 5.10), [Online]. Available: <https://physics.nist.gov/asd>, June 15, MD, National Institute of Standards and Technology, Gaithersburg, 2023, p. 2022.
- [36] A.-M. Harri, M. Genzer, O. Kemppinen, H. Kahanpää, J. Gomez-Elvira, J. A. Rodriguez-Manfredi, R. Haberle, J. Polkko, W. Schmidt, H. Savijärvi, et al., Pressure observations by the curiosity rover: initial results, *J. Geophys. Res. Planets* 119 (1) (2014) 82–92.
- [37] J. Rodriguez-Manfredi, M. de la Torre Juarez, A. Sanchez-Lavega, R. Hueso, G. Martinez, M. Lemmon, C. Newman, A. Munguira, M. Hieta, L. Tamppari, et al., The diverse meteorology of jezero crater over the first 250 sols of perseverance on mars, *Nat. Geosci.* (2023) 1–10.
- [38] NIST, *Digital Library of Mathematical Functions*, Release 1.1.9 of 2023-03-15, f. W. J. Olver, A. B. Olde Daalhuis, D. W. Lozier, B. I. Schneider, R. F. Boisvert, C. W. Clark, B. R. Miller, B. V. Saunders, H. S. Cohl, and M. A. McClain, eds. URL, <https://dlmf.nist.gov/>, 2023.
- [39] L. A. N. Laboratory, *Msl_ccam_obs.csv*. https://pds-geosciences.wustl.edu/msl/msl-m-chemcam-libs-4_5-rdr-v1/mslccm_1xxx/document/msl_ccam_obs.csv, 2023.
- [40] H.Y. McSween, G.J. Taylor, M.B. Wyatt, *Elemental composition of the martian crust*, *Science* 324 (5928) (2009) 736–739, <https://doi.org/10.1126/science.1165871>.
- [41] B. Martin, H. Manelski, R. Wiens, S. Clegg, P. Hansen, S. Schroder, B. Chide, *Libs peak broadening in soils on mars*, *LPI Contrib.* (2024) 1151.
- [42] D.W. Scott, *Multivariate Density Estimation: Theory, Practice, and Visualization*, John Wiley & Sons, 2015.
- [43] S. Maurice, S.M. Clegg, R.C. Wiens, O. Gasnault, W. Rapin, O. Forni, A. Cousin, V. Sautter, N. Mangold, L. Le Deit, et al., *Chemcam activities and discoveries during the nominal mission of the mars science laboratory in gale crater, mars*, *J. Anal. At. Spectrom.* 31 (4) (2016) 863–889.
- [44] D. Anderson, B. Ehlmann, O. Forni, S. Clegg, A. Cousin, N. Thomas, J. Lasue, D. Delapp, R. McInroy, O. Gasnault, et al., *Characterization of libs emission lines for the identification of chlorides, carbonates, and sulfates in salt/basalt mixtures for the application to msl chemcam data*, *J. Geophys. Res. Planets* 122 (4) (2017) 744–770.
- [46] P. Beck, P. Meslin, A. Fau, O. Forni, O. Gasnault, J. Lasue, A. Cousin, S. Schröder, S. Maurice, W. Rapin, R. Wiens, A. Ollila, E. Dehouck, N. Mangold, B. Garcia, S. Schwartz, W. Goetz, N. Lanza, *Detectability of carbon with chemcam libs: distinguishing sample from mars atmospheric carbon, and application to gale crater*, *Icarus* 408 (2024) 115840, <https://doi.org/10.1016/j.icarus.2023.115840>.
- [47] W. Rapin, P.-Y. Meslin, S. Maurice, R.C. Wiens, D. Laporte, B. Chauviré, O. Gasnault, S. Schröder, P. Beck, S. Bender, et al., *Quantification of water content by laser induced breakdown spectroscopy on mars*, *Spectrochim. Acta B At. Spectrosc.* 130 (2017) 82–100.
- [48] B. Chide, S. Maurice, B. Bousquet, X. Jacob, D. Mimoun, N. Murdoch, A. Cousin, G. David, J. Lasue, P.-Y. Meslin, et al., *Focusing a laser-induced breakdown spectroscopy (libs) telescope with a microphone*, in: *50th Annual Lunar and Planetary Science Conference*, 2019, p. 2296.
- [49] C. Fabre, S. Maurice, A. Cousin, R. Wiens, O. Forni, V. Sautter, D. Guillaume, *Onboard calibration igneous targets for the mars science laboratory curiosity rover and the chemistry camera laser induced breakdown spectroscopy instrument*, *Spectrochim. Acta B At. Spectrosc.* 66 (3–4) (2011) 280–289.
- [51] A. Cousin, V. Sautter, C. Fabre, G. Dromart, G. Montagnac, C. Drouet, P. Meslin, O. Gasnault, O. Beyssac, S. Bernard, et al., *Supercam calibration targets on board the perseverance rover: fabrication and quantitative characterization*, *Spectrochim. Acta B At. Spectrosc.* 188 (2022) 106341.
- [52] W. Rapin, B. Bousquet, J. Lasue, P.-Y. Meslin, J.-L. Lacour, C. Fabre, R. Wiens, J. Frydenvang, E. Dehouck, S. Maurice, O. Gasnault, O. Forni, A. Cousin, *Roughness effects on the hydrogen signal in laser-induced breakdown spectroscopy*, *Spectrochim. Acta B At. Spectrosc.* 137 (2017) 13–22, <https://doi.org/10.1016/j.sab.2017.09.003>.
- [53] S. Palanco, J. Baena, J. Laserna, *Open-path laser-induced plasma spectrometry for remote analytical measurements on solid surfaces*, *Spectrochim. Acta B At. Spectrosc.* 57 (3) (2002) 591–599, [https://doi.org/10.1016/s0584-8547\(01\)00388-3](https://doi.org/10.1016/s0584-8547(01)00388-3).
- [54] R. Brennetot, J.L. Lacour, E. Vors, A. Rivoallan, D. Vailhen, S. Maurice, *Mars analysis by laser-induced breakdown spectroscopy (malis): influence of mars atmosphere on plasma emission and study of factors influencing plasma emission with the use of doehlert designs*, *Appl. Spectrosc.* 57 (7) (2003) 744–752, <https://doi.org/10.1366/000370203322102816>.
- [55] C. López-Moreno, S. Palanco, J.J. Laserna, *Stand-off analysis of moving targets using laser-induced breakdown spectroscopy*, *J. Anal. At. Spectrom.* 22 (1) (2007) 84–87, <https://doi.org/10.1039/b609705g>.
- [56] E. Breves, K. Lepore, M. Dyar, S. Bender, R. Tokar, T. Boucher, *Laser-induced breakdown spectra of rock powders at variable ablation and collection angles under mars-analog conditions*, *Spectrochim. Acta B At. Spectrosc.* 137 (2017) 46–58, <https://doi.org/10.1016/j.sab.2017.09.002>.
- [57] Y.-Y.S. Zhao, J. Yu, G. Wei, L. Pan, X. Liu, Y. Lin, Y. Liu, C. Sun, X. Wang, J. Wang, et al., *In situ analysis of surface composition and meteorology at the zhurong landing site on mars*, *Natl. Sci. Rev.* 10 (6) (2023) nwad056.